ELSEVIER

Polymer 43 (2002) 6421–6428

polymer

www.elsevier.com/locate/polymer

Comparison of the effect of reactive and non-reactive steric stabilisers on the mechanism of film formation in methyl methacrylate/butyl acrylate copolymers latexes. Part 1. Differential scanning calorimetry, dynamic mechanical analysis and atomic force microscopy

Lynda A. Cannon, Richard A. Pethrick*

Department of Pure and Applied Chemistry, University of Strathclyde, Thomas Graham Building, 295 Cathedral Street, Glasgow G1 1XL, UK

Received 11 February 2002; received in revised form 19 April 2002; accepted 13 August 2002

Abstract

A comparison of the film forming ability of methyl methacrylate (MMA)/butyl acrylate (BA) latex copolymers stabilised by either a reactive or a non-reactive steric stabiliser are reported. The study indicates the effects of constraining the stabiliser and change of the length of the hydrophilic ethylene oxide chain on the coalescence process. Segregation and diffusion of the stabiliser from the interfacial layer into the surrounding media influences both the rate of the coalescence process and the final physical properties of the films formed. Differential scanning calorimetry (DSC) and dynamic mechanical analysis (DMA) are used to indicate the mechanism of the coalescence process and identify differences between the behaviour of these two systems. The final surface structure of the films was investigated using atomic force microscopy (AFM) and revealed the extent to which coalescence of the latex particles in the surface had occurred. © 2002 Published by Elsevier Science Ltd.

Keywords: Film formation; Differential scanning calorimetry; Mechanical, thermal analysis

1. Introduction

In a previous paper [1], the authors described the application of the DSC, DMA and AFM to the study of film formation in a series of latex emulsion systems. In study of 2-ethylhexylacrylate/MMA copolymer latexes [2], coalescence was found to depend on the glass transition temperature (T_g) of the copolymer. The film forming process in acrylic polymer latex materials has been extensively discussed by a number of authors [3–12]. A comparison of the effect of variation of chain length for latexes stabilised using nonylphenol ethoxylate (NPX) (where X designates the average chain length of the ethoxylate chain) indicated that NP20 was able to facilitate coalescence whereas NP30 and NP40 inhibited coalescence. The longer chains were able to form a crystalline structure in the interfacial region. In general, evaporation of water is the dominant rate limiting process in the initial stages of film formation, when the temperature of the latex is 20 K or more above its (T_g). When the latex is nearer to T_g of the copolymer, the rate controlling step for film formation involves deformation of the spherical emulsion particles. Evaporation rates are retarded in a latex system that can undergo extensive particle deformation [13] and correlation has been observed between the film formation characteristics and T_g of the polymer.

Reactive and non-reactive steric stabilisers may be differentiated according to their ability to be chemically incorporated into the latex material. The mixed hydrophilic–hydrophobic nature of the surfactant causes the molecules to segregate to the particle surface and the disordered poly(ethyleneoxide) (PEG) segment provides a steric barrier to coalescence of the particles when dispersed in aqueous media. As a result of chemical reaction, the reactive surfactant can become polymerised into the matrix and locked into the surface layer of the particle. This study compares the film forming behaviour of a reactive and non-reactive steric stabiliser. The two surfactants selected for investigation are:

* Corresponding author. Tel.: +44-141-548-2260; fax: +44-141-548-4822.

E-mail address: r.a.pethrick@strath.ac.uk (R.A. Pethrick).

0032-3861/02/$ - see front matter © 2002 Published by Elsevier Science Ltd.
PII: S0032-3861(02)00587-6

Table 1
Characteristics of latex materials

Latex code	%nv	MFFT (K)	Mean particle size (nm)	T_g (K) DSC	M_w	M_n
1035-RS	45	291	156	285	61,100	91,750
1035-NP20	52	291	191	287	161,500	150,500

1. Synperonic NP20 (steric)

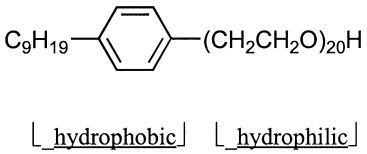

2. Reactive surfactant (steric), $n \sim 16-20$

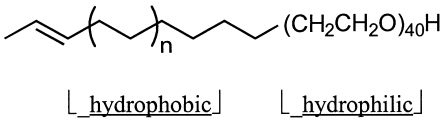

Although the hydrophobic segments are different in the above molecules, their solubility in the monomers will be very similar and will not influence significantly the initial distribution of the segments between the organic and aqueous phases. The surfactants have comparable structures, but they have different lengths of hydrophilic. The aim of the study was to determine whether the immobilisation of the surfactant and/or its chemical structure has an effect on the film formation process.

2. Experimental

2.1. Materials—latex preparation

Two different MMA/BA latex copolymers were prepared, using the method described previously [1]. The difference between the samples was the stabiliser used; in one case, it was the reactive surfactant and the other synperonic NP20. The ratio of MMA to BA was 1–3 in the reaction mixture and the total monomer content was 5% of the solution. The aqueous phase was buffered with sodium bicarbonate and polymerisation was initiated with potassium persulphate. A second seed of sodium metabisulphite was added to the reaction mixture halfway through the synthesis. The codes used to identify the polymer emulsions are 1035-RS for the reactive surfactant and 1035-NP20 for the synperonic stabilised emulsion system.

2.2. Chemical characterisation of the latex

Fourier transform infrared spectra were obtained using thin films of polymer produced by evaporation of a solution of the latex in chloroform on to a sodium chloride disc. The spectra were consistent with the monomer formulations indicated earlier. Elemental analysis of the latex films gave the following results, the theoretical values are indicated in {#}; 1035-RS: %carbon 60.77 {61.9}; %hydrogen 8.65 {8.77}; %oxygen 30.58 {29.43}. 1035-NP20: %carbon 61.88 {62.9}; %hydrogen 8.79 {7.78}; %oxygen 29.33 {29.34}. The analysis is consistent with the formulation used for the latex.

2.3. Physical characterisation of the latex film

The latex films were characterised using the following techniques.

Minimum film formation temperature (MFFT). A latex film of constant thickness was deposited using a draw bar on the heated surface of the MFFT apparatus. A defined temperature gradient was produced using a stainless steel bar heated at one end and with thermocouples distributed along its length to indicate the temperature gradient. The temperature at which a clear film is formed is defined the MFFT [14], Table 1.

Glass transition temperature (T_g). DSC measurements were performed using a Perkin–Elmer DSC-2 with a temperature scan from 243 to 403 K at 10 °C s^{-1}, using a sensitivity range of 5 mcal s^{-1}. The scans obtained were used to determine the T_g, Table 1.

Solid content of the emulsions. The initial and final weight after drying at 80 °C overnight were used to determine the percentage of non-volatiles (%nv):

$$\%\text{nv} = \frac{\text{final weight}}{\text{initial weight}} \times 100 \quad (1)$$

The samples were cooled to room temperature before reweighing in order to minimise the error in this measurement, Table 1.

Particle size determination. A Malvern Autosizer 2C, has a range of measurement of particle size from 0.00 to 3 μm, and was used to measure the particle size emulsions, Table 1.

Molecular mass determination. Gel permeation chromatography (GPC) measurements were performed by RAPRA Technology Ltd using dimethyl formamide (DMF) as solvent. A Plgel 2 X mixed bed, 30 cm, 10 μm column was used with DMF buffered with ammonium acetate as eluent at a flow rate of ml/min. The GPC system was calibrated with poly(methyl methacrylate) (PMMA) and all

the results are quoted as 'PMMA equivalent' molecular masses, Table 1.

2.4. Stage one of film formation

The transformation of emulsion into a solid film was followed by dynamic mechanical analysis.

Dynamic mechanical analysis. An adapted Rheovibron-DDV II C was used to monitor the change in mechanical properties as the substrate coated with latex dries. A no. 1 Whatmann filter paper, 9 mm × 45 mm was used as the substrate and was held between two clamps; one end connected to a stress transducer, the other to a strain gauge. A force, P, was applied to the strip of paper of length, l, and cross sectional area, A, and the stretched length was Δl. The longitudinal stress was P/A and the longitudinal strain $\Delta l/l$. The Young's modulus of the solid, E, was defined as:

$$\frac{\text{Stress}}{\text{Strain}} = \frac{P/A}{\Delta l/l} = \frac{Pl}{A\Delta l} = E \tag{2}$$

An *A/D* card in a computer monitored the strain transducer. The stress applied by the Rheovibron was fixed and the measured strain depends directly on the modulus of the sample. A 50 μl of sample of emulsion was applied to the substrate using a micropipette and the output voltage from the strain gauge monitored as a function of time until a constant value was obtained. Because the paper has a variable modulus, the traces are quoted in terms of the voltage variation with time rather than attempting to assign modulus values to the plots. Profiles were obtained at different drying temperatures. The drying rate was calculated from the slope of the plot of the voltage variation against time for a range of temperatures. The calculated rates were used to generate an Arrhenius plot

$$\ln(\Delta[\text{strain}]) = \frac{-E_a}{R}\frac{1}{T} + C \tag{3}$$

where E_a is the activation energy for the film formation process.

2.5. Stages two and three of film formation—the maturation of latex films

When the latex film is macroscopically dry, other techniques can be applied to the characterisation of the films.

Calorimetric compensation [15,16]. DSC was used to discriminate between reversible and irreversible processes occurring during drying of the latex film. The samples were cast into a flat petridish and dried for 24 h. Two samples with identical weight (± 2%) were placed in sample pans of identical weight (± 0.1 mg). The analysis was performed in three consecutive steps:

- Step 1: a temperature scan was performed on a dried latex sample measured against an empty reference pan and the scan was terminated before the latex decomposition temperature.
- Step 2: the calorimeter was cooled to ambient temperature and the original sample transferred to the reference holder. A fresh sample was placed in the first sample holder and the heating scan repeated. The sample in the reference holder will display reversible thermal changes, whereas the fresh sample in the sample holder will show both reversible and irreversible changes. Two types of irreversible change can occur, disappearance of the specific surface (coalescence) of the latex particles and destruction of crystalline regions in the film. These latex films are amorphous, however, regions of crystallinity can arise from the presence of the long chain surfactant segregating in the aqueous phase.
- Step 3: after cooling, a second run was performed to generate a base line.

This method of analysis allows identification, quantification and separation of reversible and irreversible thermal changes. The method can be applied to the measurement of the enthalpy of coalescence of latex films, the T_g and identification of crystalline domains. The data presented were obtained with 20–30 mg of material and measured over a temperature range of 243–403 K at a heating rate of 10 K min^{-1} and using a sensitivity range of 10 mcal. The first run exhibits a clear thermal step indicative of the T_g. The second run contains an exothermic peak associated with the coalescence process. Loss of residual moisture from the system, rearrangement and redistribution of the stabilised layer of the system and the ability of molecules to move across the latex interface to form a coalesced film will influence the energy of coalescence. The film forming properties will determine the enthalpy of disappearance of the interface between particles. The DSC was standardised using indium and the standard deviation of the data based on the enthalpy of fusion was 0.29%. The enthalpy of coalescence of the films obtained by these measurements is an indication of the total energy required for the disappearance of the interface.

Atomic force microscopy. A Burleigh AFM was used to investigate the change of the surface structure with ageing time. Latex samples were cast onto a silicon wafer, allowed to dry and scanned at regular intervals in time. Between analyses, the samples were covered to prevent contamination of the surface by dust and airborne particles. Statistical analysis of the image data allowed various roughness parameters to be determined. These are the root mean square of the line/surface, *Rq*, is given by

$$\sqrt{\frac{1}{N}\sum_{i}^{N}(Z_i - Z_{\text{avg}})^2} \tag{4}$$

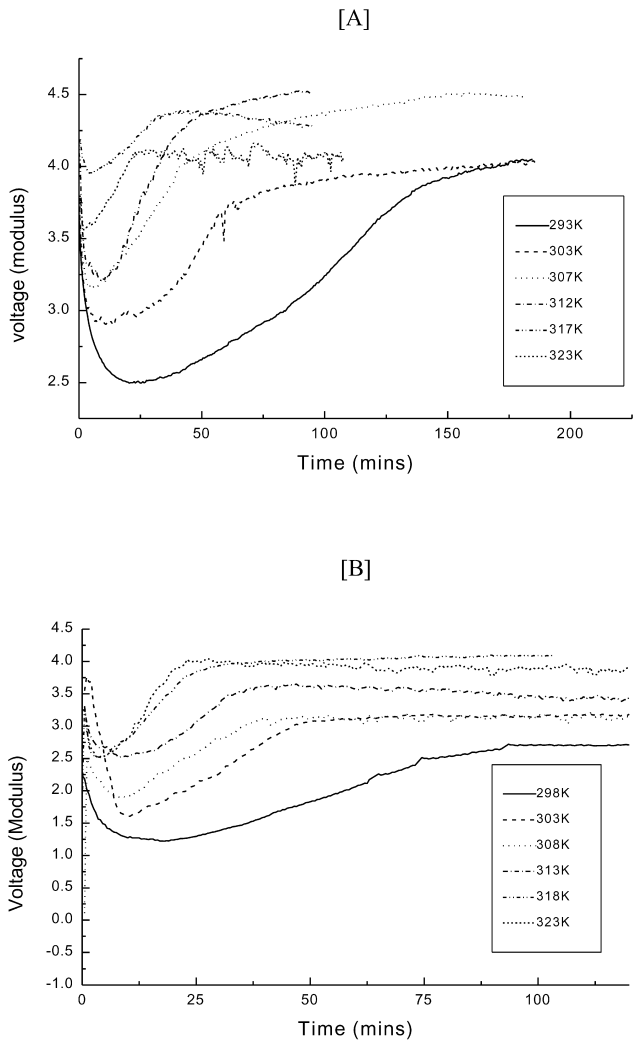

Fig. 1. Mechanical analysis of (A) 1035-RS and (B) 1035-NP20.

the height variance of the line/surface, *Ra*, is given by

$$\frac{1}{N}\sum_{i}^{N}|Z_i - Z_{\text{avg}}| \tag{5}$$

the height difference between the highest and lowest points on the line/surface $Rp - p$ given by:

$$Z_{\max} - Z_{\min} \tag{6}$$

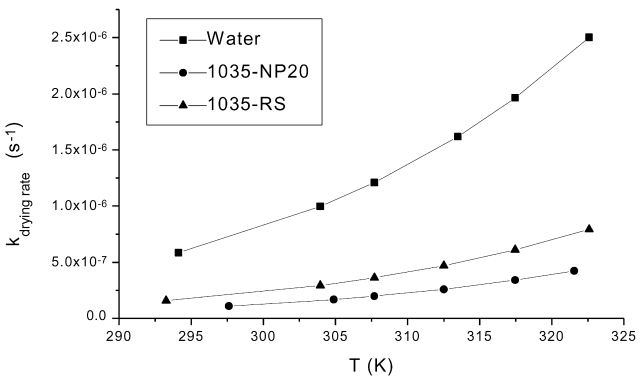

Fig. 2. Drying rate constants for 1035-RS, 1035-NP20 and water.

The mean particle size quoted in Table 1 is a mean value. The two latexes have essentially identical values of T_g and similar values of %nv indicating that these latexes should have similar physical properties. However, the latex 1035-RS has a very broad particle size distribution relative to 1035-NP20. The broader particle size distribution of 1035-RS should aid the efficiency of close packing in the drying latex.

3. Results and discussion

The analysis is divided into consideration of the drying process and the physical properties of the 'dry' latex once it has formed.

3.1. Drying process—dynamic mechanical analysis

The drying profiles for 1035-RS and 1035-NP20 were measured at temperatures between 293 and 323 K using the Rheovibron, Fig. 1. As expected for latexes with a MFFT of 291 K, a single stage drying process was observed at all temperatures. The drying profiles, Fig. 1, were used to calculate the drying rates over a range of temperatures, Fig. 2, and Arrhenius plots used to calculate the activation energies from the single stage drying process. The values of the activation energies obtained were, respectively, 40.3 ± 2.4 kJ mol^{-1} for water; 43.2 ± 2.8 kJ mol^{-1} for 1035-RS and 45.3 ± 2.6 kJ mol^{-1} for 1035-NP20. The Arrhenius plot for 1035-RS deviated from linearity at higher temperatures as a result of changes in the nature of the interactions between the PEG_{1760} in the film implying that the drying profile could be influenced by the stabiliser. The similarity of the activation energy for the drying process, indicates that water evaporation is the dominant factor in the drying process [17].

The rate constants for 1035-RS were much higher than those for NP20 and is attributed to differences in interaction in the PEG phase. As 1035-RS dries, the PEG chains will come into contact. The resultant close packing of these long PEG chains can lead to formation of a crystalline region between the latex particles that will assist in the development of mechanical properties in the film. However, these crystalline regions have a detrimental effect on further coalescence of the latex particles.

3.2. Differential scanning calorimetry—calorimetric compensation method [18–21]

Latex samples were analysed at regular intervals of time, starting at the point at which a film was first formed. The thermogram showed an exothermic peak associated with coalescence and integration of the peak observed provides

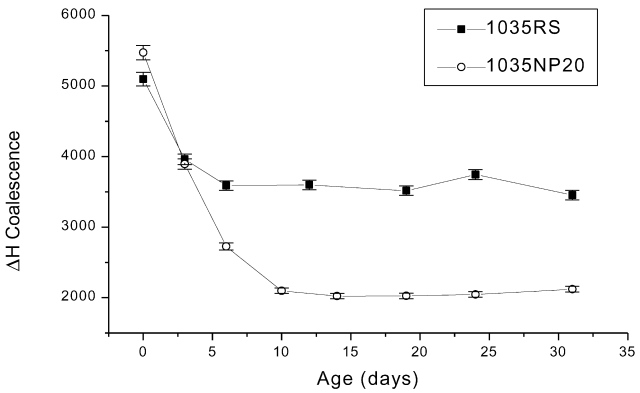

Fig. 3. Change in enthalpy of coalescence for 1035-RS and 1035-NP20.

the variation of the enthalpy of coalescence. The amount of energy required to promote coalescence in 1035-RS falls slowly in the initial stages of maturation and remains fairly constant in the latter stages, Fig. 3. For 1035-NP20, the enthalpy of coalescence falls much faster initially and again achieves a steady value in the latter stages of ageing. Approximately, 1.5 times more energy is required to promote coalescence in 1035-RS than is required for 1035-NP20. The quantitative difference between the enthalpy of coalescence for the two latexes indicates that the ability of the particles to deform and the presence of crystalline domains in the interparticulate region are influencing the energy required for coalescence. The DSC scans reveal evidence of a crystalline region in 1035-RS in the temperature range 305–330 K. The intensity of the peak increases as the sample ages. The DSC thermograms for 1035-NP20 do not contain any evidence of crystalline peaks.

3.3. Atomic force microscopy [22]

AFM of 1035-RS and 1035-NP20 was performed to obtain pictorial evidence of the coalescence process Figs. 4 and 5. Both latexes exhibit initially the close packing structure, which is typical of a spherical latex system. The films were scanned at various stages during ageing and statistical analyses were performed on the images generated. The close packed array of spheres is clearly seen in the first scan of the two latex films. The scans reveal a significant difference in the particle sizes of the two samples. Considering the particle size, analysis performed on the latexes revealed that 1035-NP20 had a relatively narrow particle size distribution with a mean particle size of 156 nm, and 1035-RS had a much broader particle size distribution and had a slightly larger particle size. The AFM scans suggest, therefore, that the latex is subject to ordering during drying, such that smaller particles are forced to the upper layer. The scans show that the spherical pattern becomes less clear as the samples age, which is consistent with coalescence.

The scans of 1035-NP20 reveal the expected changes in surface structure, there being significant loss of structure after 19 days, prior to this time the clarity of the surface features gradually diminishes. It would be reasonable to assume that the spherical pattern would still be visible during plasticisation, only after interpenetration it would disappear. From 7 to 31 days the film establishes its mechanical properties, which is facilitated by interdiffusion. It is during this time that the spherical pattern is lost and the particles lose their identities.

However, the scans of 1035-RS also indicate that coalescence has occurred, contrary to the conclusions drawn from previous experiments. It is not possible from these scans, however, to determine the extent to which true interparticle diffusion has occurred, and the scan may reflect the formation of a solid phase between the particles which contains the crystalline PEG chains. It is possible that some of the stabiliser may not have been locked into the interface and this is able to act as a plasticiser for the subsequent coalescence of the latex particles. When the surfactant has desorbed to the particle surface, it is possible that some plasticisation of the particle surface may occur leading to the disappearance of the particle interface.

The statistical quantities derived from the scans are plotted against sample age in Fig. 6. The statistics show the degree of surface roughness in the samples. The results of 1035-RS reveal a downward trend in the surface roughness as the sample ages. 1035-NP20 shows a decline in surface roughness over the first 20 days of ageing. After 20 days, the surface roughness increases; this again may be attributable to synperonic NP20. Keintz [17] studied plasticisation of latex particles by synperonic NP20 using ATR-FTIR. He showed that a small amount of synperonic NP20, equal to the solubility limit takes part in plasticisation, and the remainder is desorbed to the surface. Plasticisation by synperonic NP20 has been shown by DSC measurements. It is therefore reasonable to assume that, because of its surface-active nature, some synperonic NP20 could be segregated to the surface as the film ages. Desorption of surfactant to the film–air interface has been studied by several authors using AFM and FTIR and they have shown that peaks of surfactant can form on the film surface. It is, therefore, possible that the increase in surface roughness is a consequence of NP20 segregating to the surface.

4. Conclusions

Comparison of the behaviour observed in the drying of synperonic NP20 and the reactive surfactant reveal interesting features which reflect the influence of stabiliser structure on the coalescence process. Mechanical measurements of drying show that both latexes exhibit a single stage drying profile indicative that, at ambient temperature they are above their MFFT. The drying rates were essentially those of water evaporation.

DSC measurements of the enthalpy of coalescence

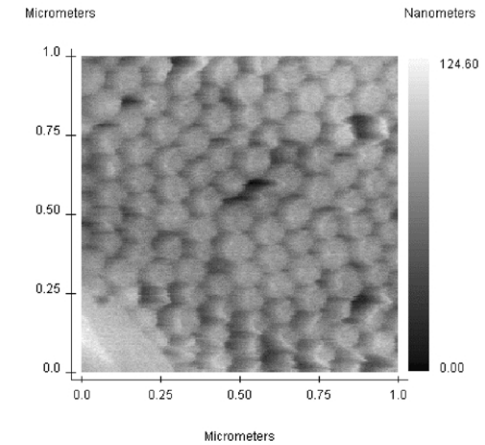

a) - zero

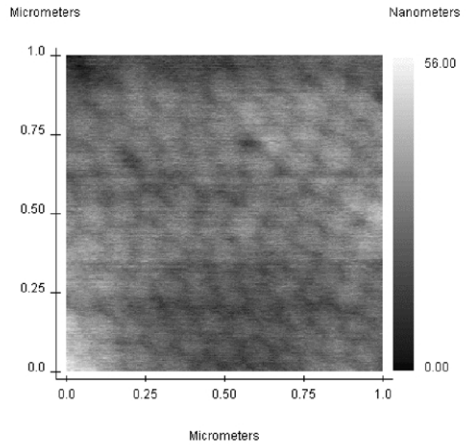

b) - 4 days

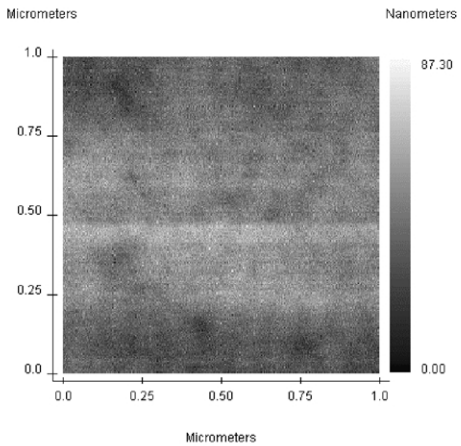

c) - 11 days

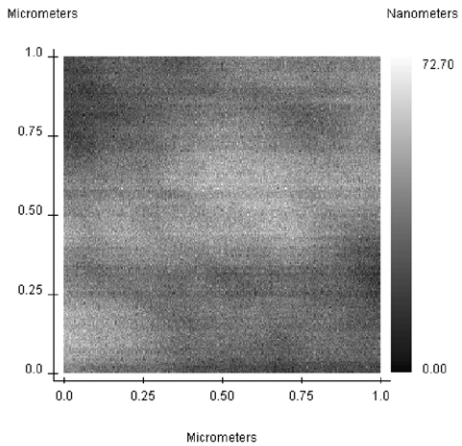

d) - 19 days

e) - 32 days

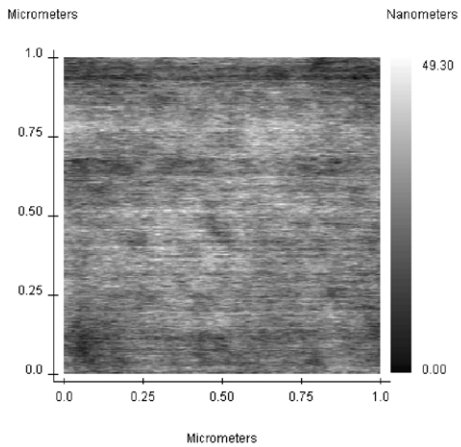

Fig. 4. AFM scans of 1035-RS.

indicate the inhibition of coalescence in 1035-RS and suggest that coalescence may not have occurred to completion in 1035-NP20. The DSC thermograms also revealed a crystalline melting peak at ~322 K which can be attributed to melting of a PEG-1760 region which would be formed by the reactive surfactant. This confirms previous suspicions that the formation of surfactant related crystalline regions were responsible for coalescence inhibition.

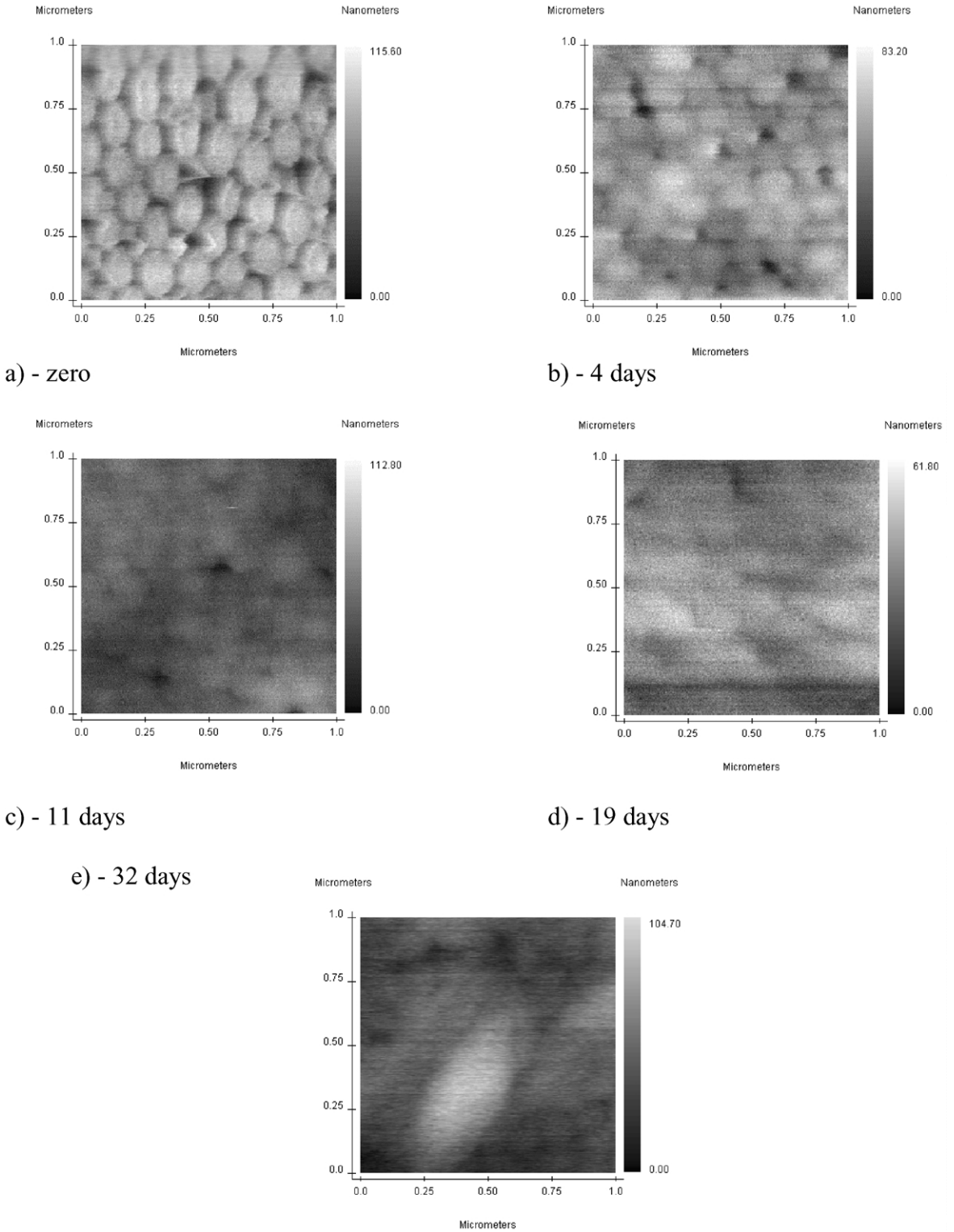

Fig. 5. AFM scans of 1035-NP20.

AFM scans of the samples revealed the classical close packed array of spheres in young samples, however, this had disappeared by 19 days in both samples. These images lend further evidence that coalescence has occurred in 1035-NP20 and that the features seen in DSC and high temperature dielectric measurements were the consequence of residual interfaces in the film. All previous results clearly show that 1035-RS had not coalesced and that coalescence is inhibited. The appearance of coalescence in the AFM images of 1035-RS can be attributed to the effects of a small

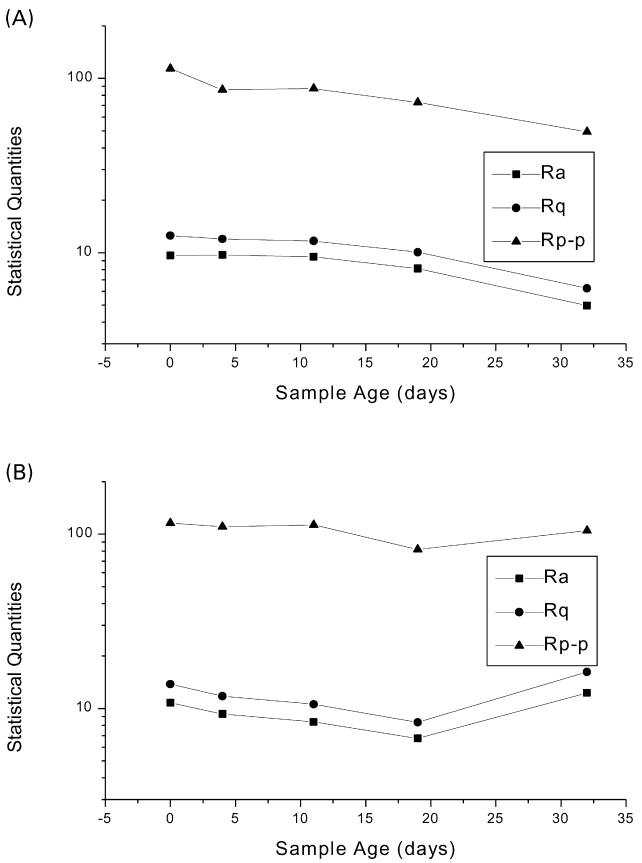

Fig. 6. Statistical analysis of (A) 1035-RS AFM scans and (B) 1035-NP20 AFM scans.

amount of 'free' stabiliser. This would desorb to the film–air interface during ageing and facilitate plasticisation of the surface layer giving the impression of a coalesced film. Part 2 describes dielectric measurements carried out on these systems and provides further insight into the coalescence process.

Acknowledgements

One of us (LC) wishes to thank the EPSRC and ICI (Paints) for the support of a CASE studentship for the period of this research. We wish to thank Dr David Taylor and Dr David Elliott for their help and guidance during the course of this study.

References

[1] Cannon LA, Pethrick RA. Polymer 2002;43:1223–33.
[2] Cannon LA, Pethrick RA. Macromolecules 1999;32:7617–29.
[3] Eckersley ST, Rudin A. Film formation in waterbourne coatings. Provder T, Winnik MA, Urban MW, editors. ACS Symp Ser 1996; 648:2.
[4] Niu BJ, Martin LR, Tebelius LK, Urban MW. Film formation in waterbourne coatings. Provder T, Winnik MA, Urban MW, editors. ACS Symp Ser 1996;648:301.
[5] Keddie JL, Meredith P, Jones RAL, Donald AM. Film formation in waterbourne coatings. Provder T, Winnik MA, Urban MW, editors. ACS Symp Ser 1996;648:332.
[6] Eu M-D, Ullman R. Film formation in waterbourne coatings. Provder T, Winnik MA, Urban MW, editors. ACS Symp Ser 1996;648:79.
[7] Winnik MA. Film formation in waterbourne coatings. Provder T, Winnik MA, Urban MW, editors. ACS Symp Ser 1996;648:51.
[8] Routgh AF, Russel WB. AICHE J 1998;44(9):2088.
[9] Feng JR, Winnik MA. Macromolecules 1997;30(15):4324.
[10] Wang YC, Winnik MA. J Phys Chem 1993;97(11):2507.
[11] Winnik MA, Winnik FM. Advances in chemistry series 236. Washington, DC: American Chemical Society; 1993. p. 485.
[12] Sperry PR, Snyder BS, O'Dowd ML, Lesko PM. Langmuir 1994;10: 2619.
[13] Keddie JL, Meredith P, Jones RAL, Donald AM. Macromolecules 1995;28:2673–82.
[14] O'Callaghan KJ, Rudin A. J Polym Sci, Part A: Polym Chem 1995; 33(11):1849–57.
[15] Rodriguez F. Principles of polymer systems, 2nd ed. New York: Wiley; 1992.
[16] Mahr TG. J Phys Chem 1970;74:2160.
[17] Keintz E, Holl Y. Colloids Surf A—Physicochem Engng Asp 1993; 78:255–70.
[18] Harkins WD. J Chem Phys 1945;13:381.
[19] Harkins WD. J Chem Phys 1946;14:47.
[20] Harkins WD. J Am Chem Soc 1947;69:1428.
[21] Harkins WD. J Polym Sci 1950;5:217.
[22] AFM reference manual, Burleigh; 1995.